BMC Plant Biology

RESEARCH Open Access

Widely targeted volatilomics and transcriptome analyses reveal the differences in volatile organic components in differently shaped *Amomum tsao-ko* fruits

Mengli Ma[1], Hongbo Fu[1], Tiantao Wang[1], Lina Xiong[1], Ping Feng[2] and Bingyue Lu[1*]

Abstract

Background *Amomum tsao-ko* is an important aromatic crop used in medicines and food. It can be categorized into three main types based on the fruit shape: long (L), oval (O), and round (R). However, limited information is available on the volatile substances present in differently shaped *A. tsao-ko* fruits. This study investigated the characteristics and biosynthesis of volatile organic compounds (VOCs) in fresh and dried *A. tsao-ko* fruits of different shapes using widely targeted volatilomics and transcriptome analyses.

Results In total, 978 VOCs, primarily terpenoids, esters, and heterocyclic compounds, were detected. The number of differentially accumulated volatile organic compounds (DAVOCs) in dried fruits of various shapes was significantly higher than that in fresh fruits, with terpenoids, esters, and heterocyclic compounds accounting for approximately 50% of the total DAVOCs. Notably, α-phellandrene, identified as a shared differential accumulated terpenoid across various fruit shapes, was detected in both fresh and dried fruits. Through transcriptome analysis, 40 candidate genes implicated in the terpenoid biosynthesis pathway were screened. An integrated analysis of the metabolome and transcriptome revealed that the structural genes *HMGR-2*, *TPS7*, *TPS5-10*, *TPS21-3*, *TPS21-5*, *TPS21-6*, *TPS21-7*, and *TPS21-9*, along with 81 transcription factors (including 17 NACs, 16 MYBs, 16 AP2/ERFs, 13 WRKYs, 13 bHLHs, and 6 bZIPs), co-regulate the biosynthesis of volatile terpenoids.

Conclusions This study expands our understanding of the volatile metabolism profile of *A. tsao-ko* and provides a solid foundation for future investigations of the mechanisms governing fruit quality.

Keywords *Amomum tsao-ko*, Volatile organic compound, Terpenoid, Widely targeted volatilomics, Transcriptome

*Correspondence:
Bingyue Lu
lby202@126.com
[1]Key Laboratory for Research and Utilization of Characteristic Biological Resources in Southern Yunnan, College of Biological and Agricultural Sciences, Honghe University, Mengzi, Yunnan 661199, China
[2]Jinping Shili Medicinal Materials Development Co., Ltd, Jinping, Yunnan 661500, China

Backgroud

Amomum tsao-ko Crevost & Lemarié is a perennial herbaceous plant belonging to the Zingiberaceae family. The dried fruits of this plant, commonly known as Caoguo in Chinese, have been utilized both as a Chinese herbal medicine and as a spice for cooking [1]. In traditional Chinese medicine, *A. tsao-ko* is primarily used to treat cold–damp internal resistance, epigastric distension and pain, fullness and vomiting, gastric dysfunction, indigestion, and other related symptoms [2]. Modern pharmacological research has demonstrated that *A. tsao-ko* possesses various pharmacological properties [3]. Moreover, *A. tsao-ko* is widely employed as a food additive due to its strong aroma and spicy taste, which imparts a unique flavor to dishes. As an edible medicinal crop, *A. tsao-ko* is rich in volatile oils and contains various active components. Various volatile oil components have been isolated from *A. tsao-ko* and identified, including monoterpenoids, sesquiterpenoids, aliphatics, aromatics, and ketones. The main ingredients are eucalyptol, citral, α-pinene, β-pinene, and limonene [3]. *A. tsao-ko* germplasm can have different shapes, including long, oval, round, and shuttle. Among these, the oval shape is the most common, followed by long and round shapes, whereas shuttle-shaped germplasms are rare [4]. Recent studies have shown a significant positive correlation between fruit shapes and the contents of various volatile substances—round fruits contain more volatile components and have a greater aroma [5, 6].

Numerous studies have demonstrated that terpenoids constitute the principal components of *A. tsao-ko* and are predominantly located in its volatile oils [7]. Terpenoids are extensively distributed in medicinal plants and manifest a diverse array of pharmacological activities, including anticancer, antioxidant, antitumor, anti-inflammatory, and immunosuppressive effects [8]. The biosynthesis of plant terpenoids occurs via two primary metabolic pathways: the mevalonic acid (MVA) pathway and the 2-C-methylerythritol 4-phosphate (MEP) pathway. The MVA pathway involves genes responsible for upstream terpenoids skeleton synthesis, including *acetyl-CoA C-acetyltransferase*, *hydroxymethylglutaryl-CoA synthase* (*HMGS*), *3-hydroxy-3-methylglotaryl-coenzyme A reductase* (*HMGR*), *mevalonate kinase*, *phosphomevalonate kinase*, and *farnesyl diphosphate synthase* (*FPPS*). The MEP pathway includes genes such as *1-deoxy-D-xylulose 5-phosphate synthase* (*DXS*), *1-deoxy-D-xylulose 5-phosphate reductoisomerase* (*DXR*), *2-C-methyl-Derythritol-4-phosphate cytidylyl transferase*, *4-(cytidine5'-diphospho)-2-C-methyl-derythritol kinase*, *2-C-methyl-Derythritol-2*, *4-cyclodiphosphate synthase*, *(E)-4-hydroxy-3-methylbut-2-en-1-yl diphosphate synthase* (*ispG*), *4-hydroxy-3-methylbut-2-(E)-enyl diphosphate reductase* (*ispH*), and *geranyl pyrophosphate synthase* (*GPPS*). Different terpenoids are produced through the *terpenoid synthase* (*TPS*) gene. Recently, the genome sequence of *A. tsao-ko* was determined [6, 9]. These sequencing results offer valuable insights into the molecular mechanisms underlying terpenoids synthesis in *A. tsao-ko*.

Previous studies on *A. tsao-ko* have primarily utilized gas chromatography–mass spectrometry (GC–MS) to detect and identify volatile substances. However, this method has limitations in terms of its sensitivity and efficiency. For example, Cui et al. [10] identified 34 chemicals in the volatile oil, with high levels of eucalyptol (34.6–37.8%), α-phellandrene (5.4–5.8%), and geraniol (4.8–5.4%). Similarly, 73 compounds were found in *A. tsao-ko* essential oil, mainly eucalyptol (45.24%), geraniol (5.11%), α-terpineol (3.59%), and α-phellandrene (3.07%) [11]. Another study using GC–MS identified 43 compounds in the volatile oil, with eucalyptol (23.87%) and limonene (22.77%) as the major components [12]. However, with advancements in metabolome detection technology, the number of detected metabolites has significantly increased. An untargeted volatile metabolome approach has also been used to detect 200 volatile substances in *A. tsao-ko* [6]. Recently, a more advanced widely targeted volatilomics (WTV) approach was developed [13], which has enhanced detection sensitivity and has been successfully applied to various plants, such as tea [14, 15], *Opisthopappus taihangensis* [16], and *Dendrobium chrysotoxum* [17].

Although previous studies have examined the volatile oil content and components of *A. tsao-ko*, the detection of these substances has been limited and the sensitivity of the tests has been poor. In this study, we focused on long, oval, and round *A. tsao-ko* fruits, which exhibited distinct differences. We used the WTV method to analyze variations in aroma components and the volatile organic compound (VOC) content. Additionally, we conducted a transcriptome analysis to elucidate the molecular mechanisms underlying the differences in aroma. By integrating the metabolome and transcriptome data, we identified key genes involved in the synthesis of volatile metabolites. Our findings enhance the understanding of the molecular regulatory network associated with VOC synthesis and offer potential targets for future metabolic engineering aimed at improving the quality of *A. tsao-ko*.

Materials and methods

Plant material and sample collection

Three *A. tsao-ko* accessions were selected based on the fresh fruit length-to-width ratio (LWR) to represent different fruit shapes: long (LWR > 1.8), oval (1.8 > LWR > 1.1), and round (1.1 > LWR > 0.9) (Fig. 1). A voucher specimen (H22129385, H22129388, H22129391) has been deposited in the herbarium of Honghe

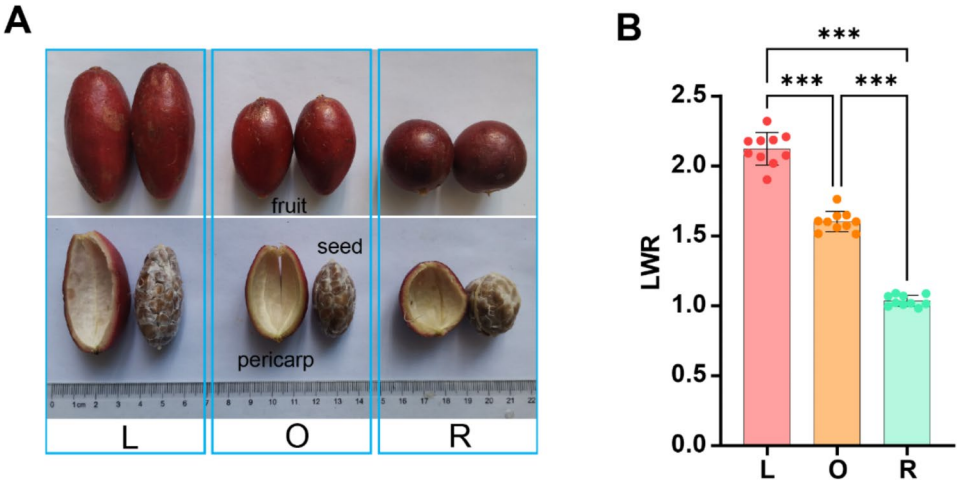

Fig. 1 Fruit phenotypes (**A**) and length-to-width ratio (LWR) (**B**) of different fruit shapes in *A. tsao-ko*. L, long shape (LWR > 1.8); O, oval shape (1.8 > LWR > 1.1); R, round shape (1.1 > LWR > 0.9). *** indicates $p < 0.001$

University, China. The abbreviations used for the fresh and dried fruits are as follows: long accessions, L1 (fresh) and L2 (dried); oval accessions, O1 (fresh) and O2 (dried); and round accessions, R1 (fresh) and R2 (dried). Ripened fruit samples were collected from Xinfazhai village, Dazhai Township County, Jinping Yao-Dai Autonomous County, Honghe Hani and Yi Autonomous Prefecture, Yunnan Province, China (22°88′78′′N, 103°33′E, 1,755 m) on October 21, 2022. The fruits of three different plants were taken from each accession. Twenty fruits from each plant were removed pericarps, and 10 fruits were mixed into one sample, which was immediately treated with liquid nitrogen. The other 10 fruits were dried at 80 °C for 48 h and then mixed into one sample. Three biological replicates were used to test each sample. A VOC analysis was performed on the fresh and dried fruit samples, and RNA sequencing (RNA-seq) was conducted on the fresh fruit samples.

Volatile extraction and widely targeted volatileomics analysis

A WTV analysis was performed as per Yuan et al. [13]. Each *A. tsao-ko* sample was powdered with liquid nitrogen, and 500 mg of the powder was placed in a 20 mL headspace vial with NaCl saturated solution to prevent enzymatic reactions. The vials were sealed with crimp-top caps and TFE-silicone septa (Agilent). For headspace SPME analysis, each vial was incubated at 60 °C for 5 min. A 120 μm DVB/CWR/PDMS fiber (Agilent) was exposed to the sample headspace for 15 min at 60 °C. VOCs were desorbed from the fiber in the GC injection port (Model 8890; Agilent) at 250 °C for 5 min in splitless mode. VOCs were identified and quantified using an Agilent Model 8890 GC and a 7000D mass spectrometer with a 30 m × 0.25 mm × 0.25 μm DB-5MS capillary column. Helium served as the carrier gas at 1.2 mL/min. The injector was kept at 250 °C and the detector at 280 °C. The oven temperature started at 40 °C for 3.5 min, then increased by 10 °C/min to 100 °C, 7 °C/min to 180 °C, and 25 °C/min to 280 °C, where it was held for 5 min. Mass spectra were recorded in electron impact ionization mode at 70 eV. The quadrupole mass detector, ion source, and transfer line were set at 150 °C, 230 °C, and 280 °C, respectively. The mass spectrometer operated in selected ion monitoring mode for identification and quantification. Volatile compounds were identified by matching their mass spectra with NIST20 and MWGCSIM1 databases. Qualitative analysis used workflow B.08.00, while quantitative analysis employed MassHunter software. Data processing was standardized with 3-hexanone-2,2,4,4-d4 (CAS: 24588-54-3) as the internal standard. The relative content (μg/g) of volatile components was calculated using the formula: Content (μg/g) = (target volatile component peak area × internal standard mass (μg)) / (internal standard peak area × sample mass (g)) [18]. Volatileomic data were analyzed using the Orthogonal Partial Least Squares Discriminant Analysis (OPLS-DA) model. Variable importance in projection (VIP) values of the metabolites were extracted from the OPLS-DA results. Differentially accumulated volatile organic compounds (DAVOCs) between groups were identified based on VIP values (VIP ≥ 1) and log2 fold change (|log2 fold change| ≥ 1.0).

RNA extraction, cDNA library construction, and transcriptome analysis

Total RNA was extracted from the seeds of *A. tsao-ko* using TRIzol reagent (Invitrogen, USA), following the manufacturer's protocol. The RNA-seq library was subsequently constructed by Wuhan Metware Biotechnology Co., Ltd. (www.metware.cn; Wuhan, China) and sequenced on an Illumina HiSeq 2000 platform. Three

biological replicates were prepared for each fruit shape for a transcriptome analysis. The clean reads obtained after rapid filtering (version 0.18.0) [19] were aligned to the *A. tsao-ko* genome using HISAT2.2.4 [20] and Bowtie2 (https://iris.angers.inra.fr/gddh13/index.html) [6]. Novel genes and transcription factors were predicted utilizing StringTie and Itak software, respectively. The RESM software facilitated the calculation of fragments per kilobase of transcript per million mapped reads (FPKM) [21]. Differentially expressed genes (DEGs) were identified using cutoff values of log2 (fold change) ≥ 1 and $P \leq 0.05$. Enrichment analysis of the DEGs was conducted employing the Kyoto Encyclopedia of Genes and Genomes (KEGG) database. The RNA-seq data have been deposited in the NCBI database under accession number PRJNA1072740.

qRT-PCR analysis

To ensure the reliability of the RNA-seq data, we conducted the real-time fluorescence quantitative RT-PCR expression verification of 12 DEGs involved in the terpenoid metabolism pathway. The internal reference gene *UBCE2* was selected, and primers were designed using the online primer design tool Primer-BLAST (Table S1). Amplification was performed using an ABI7500 quantitative PCR instrument (7500; ABI, USA). Each sample was subjected to qRT-PCR in triplicate. The relative expression levels of the DEGs in the three fruit shapes were calculated using the $2^{-\Delta\Delta Ct}$ method, L1 was defined as the control group.

Integrative analysis of the transcriptome and metabolome

To conduct a comprehensive analysis of terpenoid metabolism in *A. tsao-ko*, co-expression networks were constructed using the weighted gene co-expression network analysis (WGCNA) package in R (v4.2.2). The parameters were set as follows: networkType = sign, minModuleSize = 50, powerEstimate = 18, and MergeCutHeight = 0.25. Modules linked to differentially accumulated terpenoids (DATs) were identified with $p < 0.05$ and absolute correlation coefficients > 0.8. The network connections of structural genes, transcription factors (TFs) and metabolites in key modules were visualized using Cytoscape (v3.9.1).

Results

Identification of volatile organic compounds in *A. tsao-ko*

To comprehensively understand the types and contents of volatile substances in *A. tsao-ko*, we employed WTV to detect metabolites in the three different fruit shapes before and after drying. In total, 978 VOCs were identified, including terpenoids, alcohols, ketones, heterocyclic compounds, hydrocarbons, aromatics, aldehydes, esters, phenols, and acids (Fig. 2A). Terpenoids were the most abundant, comprising 19.92% (195 compounds) of the identified VOCs, followed by esters (16.24%, 159 compounds) and heterocyclic compounds (15.83%, 155 compounds). When considering the contents of different substances, terpenoids also emerged as the most abundant category across all samples, constituting between 27.44% (R1) and 31.52% (L1) of the total VOCs (Fig. 2B). Among the top ten VOCs in each sample, the contents of eucalyptol and β-phellandrene were higher (Fig. 2C). Furthermore, monoterpenoids such as citral, D-limonene, and pseudolimonene, were also identified as significant components (Fig. 2C). Consequently, volatile terpenoids play a crucial role in shaping the distinctive aroma of *A. tsao-ko*.

The principal component analysis (PCA) results are presented in Fig. 3A. PC1 and PC2 explained 36.84% and 23.35% of the observed variations, respectively. The samples from each group showed strong clustering patterns. Notably, there was a more noticeable difference in the VOCs content of dried fruits compared with fresh fruits. The VOC profiles of the fruits before and after drying were significantly different. Additionally, the hierarchical clustering analysis effectively separated the samples into six distinct groups and indicated significant variations in the VOCs between the different samples (Fig. 3B).

Differentially accumulated volatile organic compounds in differently shaped *A. tsao-ko* fruits

Nine groups were subjected to a pairwise comparison to clarify differences in VOCs among samples of different fruit shapes in *A. tsao-ko* (Fig. 4A). A total of 167 (62 upregulated and 105 downregulated), 154 (41 upregulated and 113 downregulated), and 101 (30 upregulated and 71 downregulated) DAVOCs were identified in L1 vs. O1, L1 vs. R1, and O1 vs. R1, respectively. The majority consisted of heterocyclic compounds, terpenoids, and ester compounds (Fig. S1). Notably, the number of DAVOCs was significantly higher in the differently shaped dried fruits than in the fresh fruits (Fig. 4A). These DAVOCs of the dried fruits mainly included terpenoids, esters, and heterocyclic compounds, which accounted for approximately 50% of the total DAVOCs (Fig. S1).

We focused on the DAVOCs involved in terpenoids. A total of 28, 23, and 14 differentially accumulated terpenoids (DATs) were identified between L1 and O1, L1 and R1, and O1 and R1, respectively (Fig. 4B). Among them, monoterpenoids (34) were the main DATs, followed by sesquiterpenoids (6) (Table S2). Figure 4C presents a heatmap illustrating the accumulation patterns of the DATs in the three fruit types. Thirteen DATs were more abundant in L1, including α-terpinene, β-pinene, α-phellandrene, and terpinolene. It was noteworthy that the contents of three sesquiterpenes (petasitene, β-elemene, and Bicyclo[5.2.0]nonane, 2-methylene-4,8,8-trimethyl-4-vinyl-)

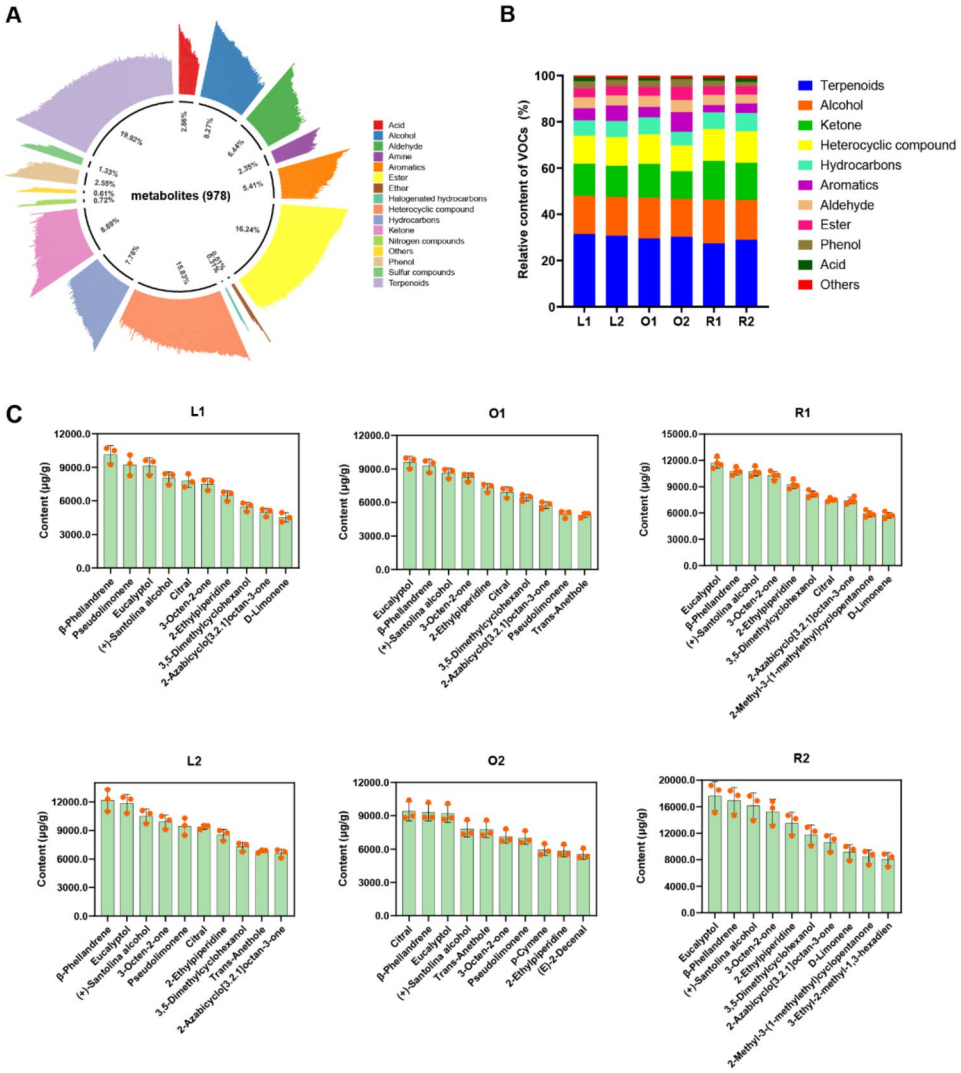

Fig. 2 Identification of volatile organic compounds in *A. tsao-ko*. Classification chart for all volatile organic compounds (VOCs) (**A**); the relative content percentage of different types of VOCs; L1, long fresh fruit; L2, long dry fruit; O1, oval fresh fruit; O2, oval dry fruit; R1, round fresh fruit; R2, round dry fruit (**B**); relative content of the top 10 VOCs in differently shaped fruits (**C**)

were higher in O1. Conversely, R1 exhibited greater abundances of 2,6-dimethyl-2,4,6-octatriene, cosmene, (+)-limonene oxide, (Z)-2,2-Dimethyl-3-(3-methyl-penta-2,4-dien-1-yl)oxirane, carveol, trans-carveol, 1-terpinenol, (+/-)-isoborneol, 2-Oxabicyclo[2.2.2]octan-6-one, and 1,3,3-trimethyl-. Terpinolene, rose oxide, and α-phellandrene exhibited significant differences among the different fruit shapes and were shared DATs among the fresh fruits. More DATs were detected in dried fruits compared with fresh fruits; there were 57, 47, and 48 DATs in the comparisons between L2 and O2, L2 and R2, and O2 and R2, respectively (Fig. 4D-E, Table S3). Notably, α-phellandrene, which was consistently present as a shared DAT, was also detected in dried fruits. This suggests that α-phellandrene may serve as a potential signature metabolite for distinguishing different fruit types of *A. tsao-ko*.

DAVOCs of *A. tsao-ko* before and after drying

Significant changes were observed in the contents of various VOCs before and after drying *A. tsao-ko*. A total of 194, 363, and 266 DAVOCs were identified in L1 vs. L2, O1 vs. O2, and R1 vs. R2, respectively. These DAVOCs primarily consisted of terpenoids, esters, heterocyclic compounds, and ketones (Fig. 5A, Table S4). A Venn diagram was constructed to illustrate the number of DAVOCs unique or shared between each comparison (Fig. 5B). A total of 78 shared DAVOCs were detected, mainly including esters (24.36%), heterocyclic compounds (15.38%), terpenoids (10.25%), alcohols (8.97%), aldehydes (8.97%), and ketones (7.69%)

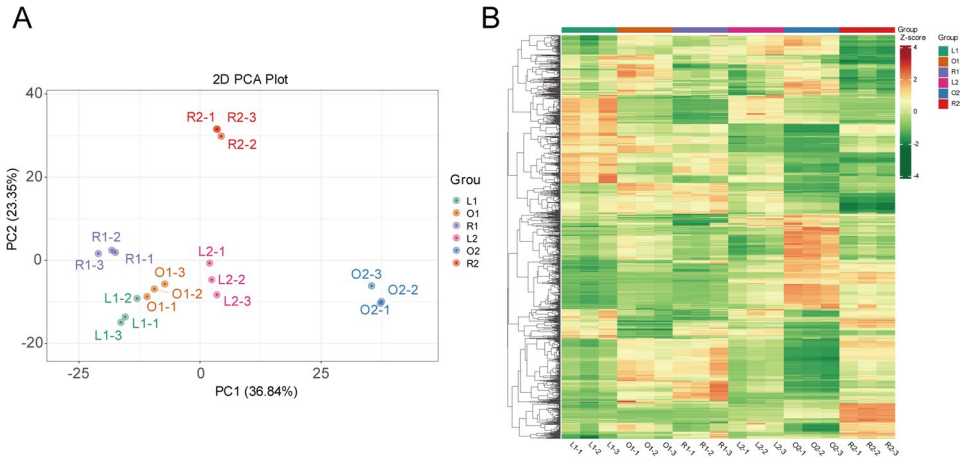

Fig. 3 Principal component analysis (PCA) plot (**A**) and clustering heatmap (**B**) of different samples of *A. tsao-ko*. L1, long fresh fruit; O1, oval fresh fruit; R1, round fresh fruit; L2, long dry fruit; O2, oval dry fruit; R2, round dry fruit. The clustering heatmap and PCA were performed using 978 volatile organic compounds (VOCs) in *A. tsao-ko*

(Fig. 5C, Table S5). Based on their relative contents, the contents of 12 shared DAVOCs significantly decreased in the dried fruits, whereas those of 66 shared DAVOCs significantly increased (Fig. 5D–F). To visualize the fold difference, a bar chart was created using the top 20 DAVOCs (Fig. 5G–I). The largest upregulated metabolite in each comparison group was 2-pentyl-2-cyclopenten-1-one (D294), and the largest downregulated metabolite was cis −9-tetradecen-1-ol (D399) in L1 vs. L2 and R1 vs. R2. In the O1 vs. O2 comparison, 3,4-dihydroxybenzaldehyde (NMW0254) exhibited the greatest downregulation. Among the three comparison groups, 2-pentyl-2-cyclopenten-1-one (D294), 1 H-pyrazole (NMW0772), (E)-4-hexen-1-ol (XMW1116), 2-pentenenitrile, 4,4-dimethyl- (XMW0779), 3(2 H)-pyridazinone (XMW0886), 4-isothiocyanatobut-1-ene (D378), 5,5-dimethyl-1,4-dihydropyrazole (XMW0149), isomaltol (XMW1454), cyclofeuchene (XMW0518), and cis −9-tetradecen-1-ol (D399) were identified as shared DAVOCs in the top 20 differential metabolites. These shared DAVOCs may explain the differences in the aromas of fresh and dried fruits.

RNA-seq of differently shaped *A. tsao-ko* fruits

To investigate the molecular basis by which volatile substances change among the differently shaped *A. tsao-ko* fruits, a transcriptome analysis was conducted on various fruit types. The clean reads obtained from each sample ranged from 6.03 to 6.73 Gb, with Q30 scores of clean bases exceeding 93.33%. The sequences matched the reference genome by 93.76%, 90.28%, and 89.04% for L1, O1, and R1, respectively, thus confirming the reliability of our transcriptomic data (Table S6).

The PCA results clearly demonstrated that the first two principal components (PC1 and PC2) effectively distinguished the three fruit shapes of *A. tsao-ko* (Fig. 6A). Furthermore, a correlation heatmap analysis revealed strong correlations between the biological replicates (Fig. 6B). By applying |log2Fold Change|≥1 and FDR≥0.05 as the filtering criteria for the DEGs, 3793 DEGs were identified in L1 vs. O1, including 2010 upregulated and 1783 downregulated genes. Similarly, there were 3848 (1734 upregulated and 2114 downregulated) and 4254 (1835 upregulated and 2419 downregulated) genes in the O1 vs. R1 and L1 vs. R1 groups, respectively (Fig. S2). To explore the functions of DEGs, KEGG analysis was performed (Fig. 6C, Table S7). A total of 25 KEGG pathways were significantly enriched (q value≤0.05) in L1 vs. O1. Many of these pathways are closely related to metabolism, including metabolic pathways (ko01100), starch and sucrose metabolism (ko00500), and biosynthesis of various plant secondary metabolites (ko00999). In contrast, there were 38 and 40 pathways significantly enriched (q value≤0.05) in L1 vs. R1 and O1 vs. R1, respectively. These pathways mainly included metabolic pathways (ko01100), starch and sucrose metabolism (ko00500), and biosynthesis of secondary metabolites (ko01110). Interestingly, we noticed that terpenoid backbone biosynthesis (ko00900) pathway was also significantly enriched between L1 and R1 (17 genes), and between O1 and R1(18 genes).

The DEGs involved in the terpenoid backbone biosynthesis pathway (ko00900) included 1 *HMGS*, 2 *HMGR*, 6 *DXS*, 1 *DXR*, 2 *ispG*, 2 *ispH*, 1 *IDI*, 1 *FPPS*, and 2 *GGPPS* (Fig. 7, Table S8). Furthermore, two monoterpene synthase genes (*TPS7* and *TPS8*), 20 sesquiterpene synthase genes (*TPS5-1*–*TPS5-11*, and *TPS21-1*–*TPS21-9*) were identified in monoterpenoid biosynthesis (ko00902), and sesquiterpenoid and triterpenoid biosynthesis (ko00909) with FPKM≥1(Fig. 7, Table S8). Among these terpenoid biosynthesis-related genes, *DXS-4*, *ispG-2*, *TPS7*, *TPS5-1*, *TPS5-10*, and *TPS21-1* were highly expressed

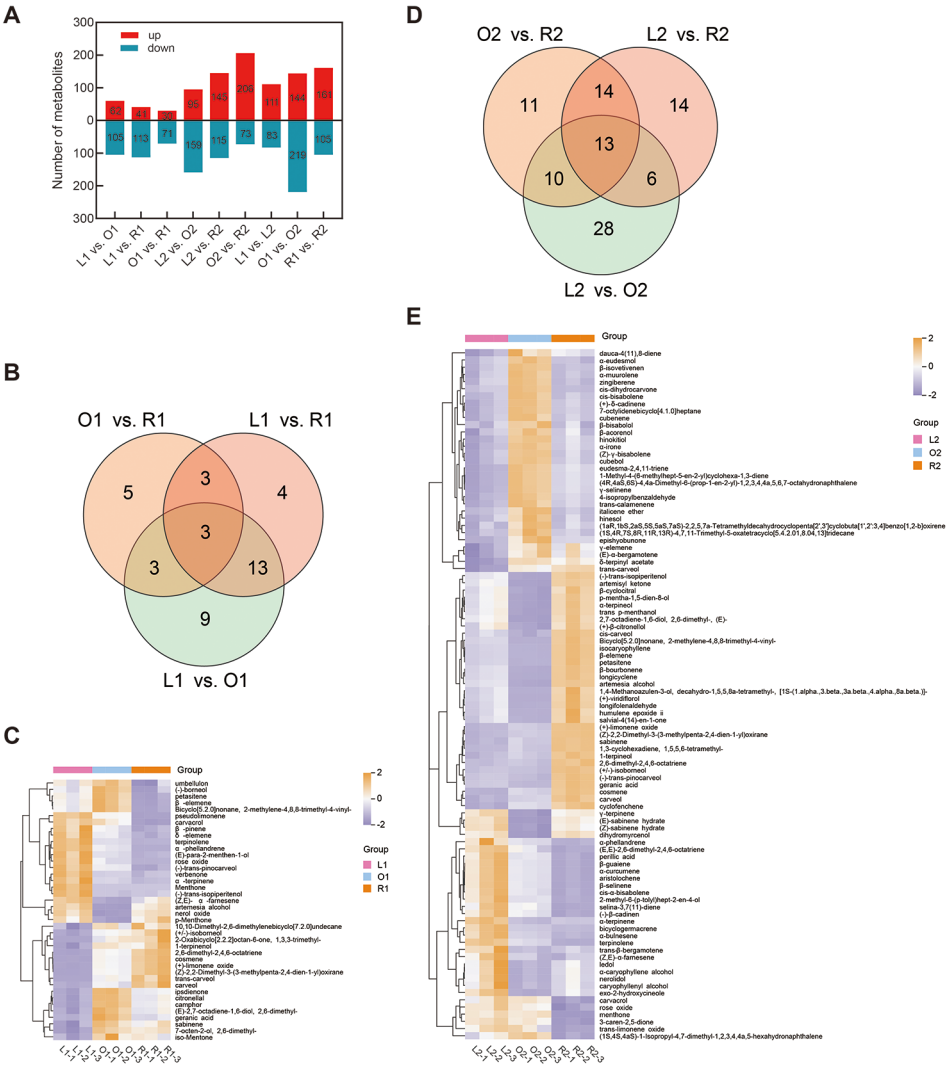

Fig. 4 Differentially accumulated volatile organic compounds (DAVOCs) and differential accumulated terpenoids (DATs) in *A. tsao-ko*. Overview of DAVOCs between two comparison groups (**A**); Venn diagram (**B**) and heatmaps (**C**) of the DATs in three comparison groups of fresh fruit; Venn diagram (**D**) and heatmaps (**E**) of the DATs in three comparison groups of dry fruit

in L1, whereas *HMGR-2*, *DXR*, *TPS5-4*, *TPS5-5*, *TPS5-6*, *TPS5-8*, *TPS5-9*, *TPS5-11*, *TPS21-1*, *TPS21-3*, *TPS21-5*, *TPS21-6*, *TPS21-7*, *TPS21-8*, and *TPS21-9* were highly expressed in O1. The remaining 19 genes were highly expressed in R1 (Fig. 7B). We selected 12 DEGs related to terpenoid biosynthesis in different fruit shapes for qRT-PCR verification. Their expression levels were consistent with the RNA-seq results (Fig. S3).

Combined transcriptome and metabolome analysis

To further explore the possible association between volatile terpenoids and gene expression, a weighted gene co-expression network analysis (WGCNA) was constructed using 6378 DEGs. A thresholding power of 18 was chosen to best fit the scale-free topology index, identifying six modules after dynamic analysis merging (Fig. 8A). The turquoise module had the most genes (1463), while the red module had the fewest (597) (Fig. 8B). The turquoise and brown modules showed significant positive correlations with most monoterpenoid profiles, suggesting their genes are crucial for monoterpenoid biosynthesis in *A. tsao-ko* (Fig. 8B). The blue module displayed strong positive correlation with sesquiterpene contents, including β-elemene (KMW0537), petasitene (XMW0964), and Bicyclo[5.2.0]nonane, 2-methylene-4,8,8-trimethyl-4-vinyl- (XMW0379) (Fig. 8B). After KEGG enrichment analysis (Fig. S4), the turquoise and blue modules were significantly enriched in metabolic pathways (ko01100) and biosynthesis of secondary metabolites (ko01110). In contrast, the brown module was predominantly enriched in metabolic pathways (ko01100) and plant hormone signal transduction (ko04075).

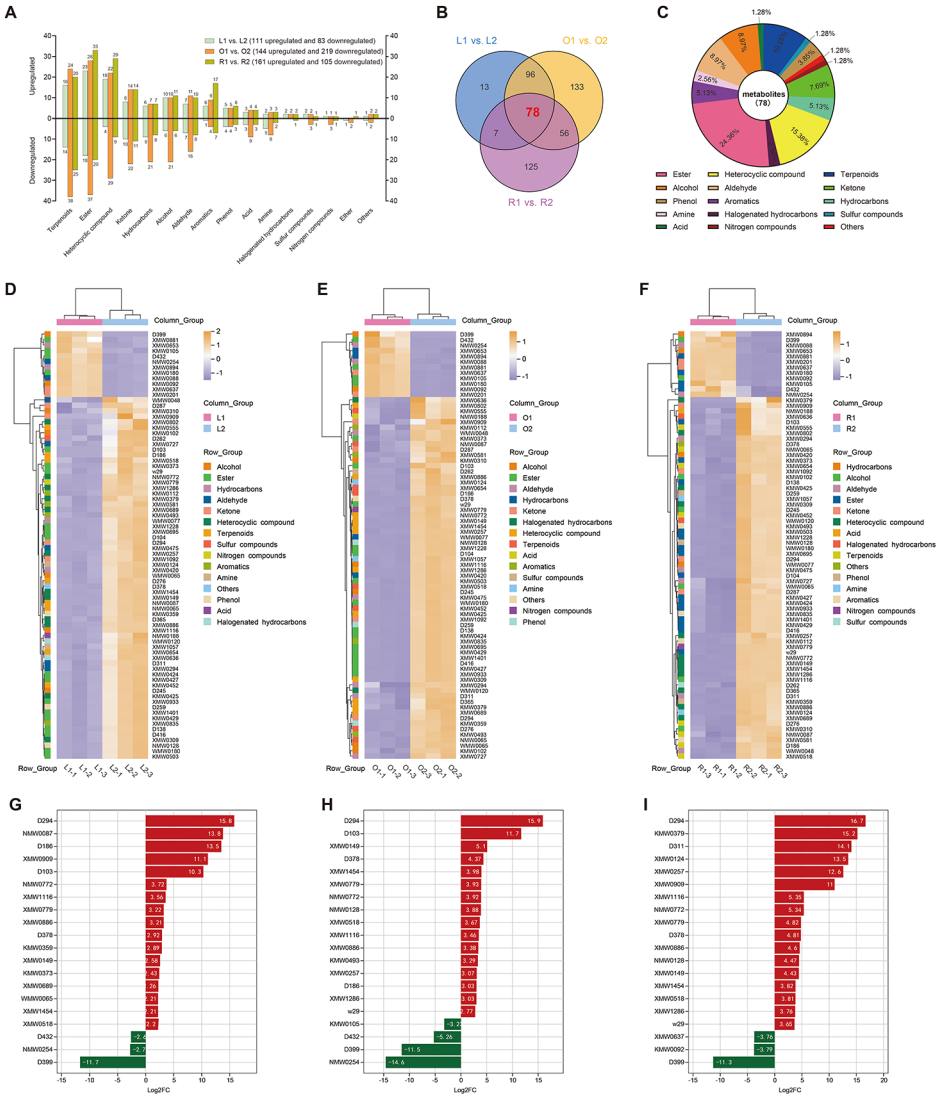

Fig. 5 DAVOC analysis of *A. tsao-ko* before and after drying. The number of DAVOCs in different groups (**A**); Venn diagram of DAVOCs in different fruit shapes (**B**); Classification chart for 78 shared DAVOCs (**C**); Heatmaps of shared DAVOCs in L1 vs. L2 (**D**), O1 vs. O2 (**E**), and R1 vs. R2 (**F**); Top 20 DAVOCs in L1 vs. L2 (**G**), O1 vs. O2 (**H**), and R1 vs. R2 (**I**). The abscissa is the log2FC of the DAVOCs, and the ordinate is the DAVOCs. The red color represents the upregulation of DAVOCs, and green represents the downregulation of DAVOCs

It is noteworthy that genes involved in the terpenoid synthesis pathway were identified within the turquoise, blue, and brown modules as follows: three genes (*DXS-4*, *TPS7*, and *TPS5-10*) in the turquoise, six genes (*HMGR-2*, *TPS5-5*, *TPS21-1*, *TPS21-5*, *TPS21-6*, and *TPS21-7*) in the blue, and eight genes (*TPS5-4*, *TPS5-6*, *TPS5-8*, *TPS5-9*, *TPS5-11*, *TPS21-3*, *TPS21-8*, and *TPS21-9*) in the brown (Table S9). Notably, *TPS7* showed strong positive correlations with pseudolimonene (XMW0709), α-phellandrene (KMW0198), and terpinolene (KMW0296), whereas *TPS5-10* exhibited strong positive correlations with pseudolimonene (XMW0709), α-phellandrene (KMW0198), terpinolene (KMW0296), β-pinene (KMW0193), and δ-elemene (KMW0509) within the turquoise module (Fig. 8C). In the blue module, *HMGR-2*, *TPS21-6*, and *TPS21-7* exhibited highly positive correlations with three sesquiterpenes (petasitene (XMW0964), β-elemene (KMW0537), and Bicyclo[5.2.0]nonane, 2-methylene-4,8,8-trimethyl-4-vinyl- (XMW0379)) and one monoterpenoid ((-)-borneol (NMW0065)) (Fig. 8C). Additionally, a significant positive correlation was observed between the *TPS21-9* in the brown module and five monoterpenoids (Fig. 8C).

Previous research indicates that AP2/ERF, NAC, WRKY, bHLH, MYB, and bZIP transcription factor families are involved in terpenoid biosynthesis [22]. A total of 47, 30, and 4 differentially expressed TF genes (with at least one sample FPKM ≥ 10) were included in

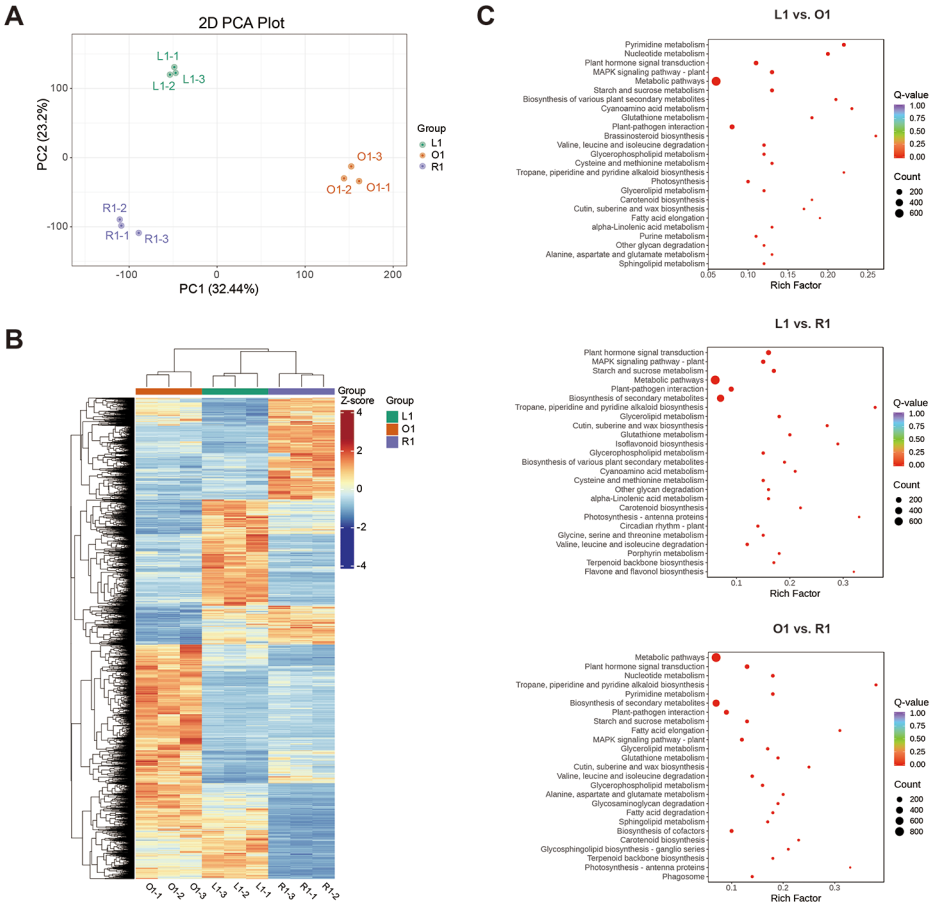

Fig. 6 Transcriptome data analysis in three *A. tsao-ko* accessions. Principal component analysis (PCA) (**A**), heatmap (**B**), and KEGG pathway enrichment analysis between L1 and O1, between L1 and R1, and between O1 and R1, respectively (**C**)

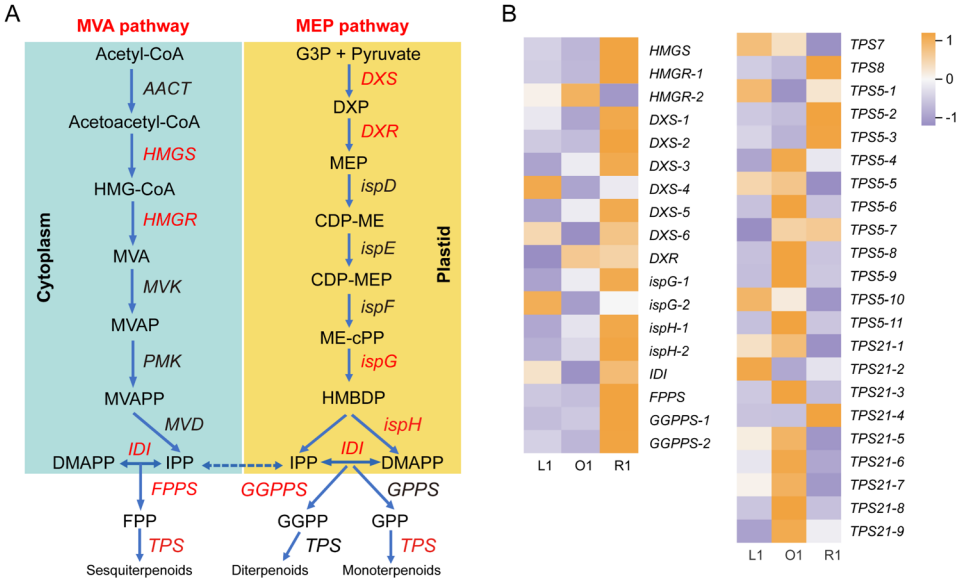

Fig. 7 Differentially expressed genes (DEGs) involved in terpenoid metabolic pathways of the different fruit shapes. Terpenoid metabolic pathways, genes significantly differentially expressed were marked red (**A**). Heatmap of the relative expression of DEGs related to terpenoid metabolic pathways (**B**)

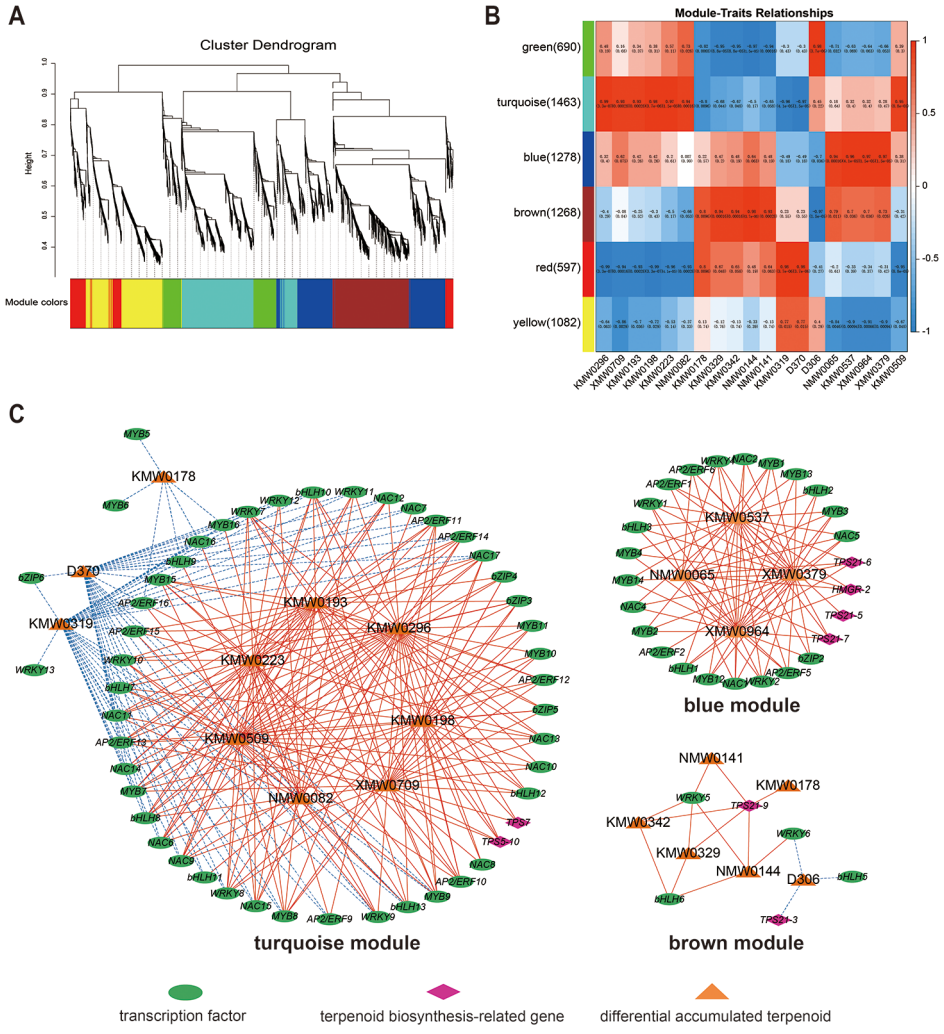

Fig. 8 Weighted gene co-expression network analysis (WGCNA) of DATs in *A. tsao-ko*. Hierarchical clustering tree using the topological overlap dissimilarity, tree branches have been colored by module membership (**A**). Module-trait relationship heatmap for 19 DATs and gene modules (**B**). KMW0296, terpinolene; XMW0709, pseudolimonene; KMW0193, β-pinene; KMW0198, α-phellandrene; KMW0223, α-terpinene; NMW0082, (-)-trans-isopiperitenol; KMW0178, sabinene; KMW0329, camphor; KMW0342, citronellal; NMW0144, geranic acid; NMW0141, (E)-2,7-octadiene-1,6-diol, 2,6-dimethyl-; KMW0319, (+)-limonene oxide; D370, (Z)-2,2-Dimethyl-3-(3-methylpenta-2,4-dien-1-yl)oxirane; D306, artemesia alcohol; NMW0065, (-)-borneol; KMW0537, β-elemene; XMW0964, petasitene; XMW0379, Bicyclo[5.2.0]nonane, 2-methylene-4,8,8-trimethyl-4-vinyl-; KMW0509, δ-elemene. The numbers in each box are the correlation coefficients (top) and p-values (bottom). Co-expression network of terpenoid biosynthesis-related genes, TFs, and DATs in turquoise module, blue module, and brown module by Cytoscape (**C**). The green oval represents TFs, the purple rhombus represents terpenoid biosynthesis-related genes, the orange triangle represents DATs. The red-solid line represents positive correlation and the blue-dashed line represents negative correlation ($|r| > 0.90$, $p < 0.01$)

the turquoise, blue, and brown modules, respectively (Table S10). Among them, the *NAC6* belonging to the turquoise module exhibited the highest expression, suggesting a potential positive regulatory effect on the levels of β-pinene (KMW0193), terpinolene (KMW0296), α-terpinene (KMW0223), (-)-trans-isopiperitenol (NMW0082), and δ-elemene (KMW0509), and a negative regulatory effect on the levels of (+)-limonene oxide (KMW0319) and (Z)-2,2-Dimethyl-3-(3-methylpenta-2,4-dien-1-yl)oxirane (D370) (Fig. 8C). Additionally, the *AP2/ERF1*, which is highly expressed within the blue module, may play a positive regulatory role in the content of three sesquiterpenes: β-elemene (KMW0537), petasitene (XMW0964), and Bicyclo[5.2.0]nonane, 2-methylene-4,8,8-trimethyl-4-vinyl- (XMW0379) (Fig. 8C). As a shared DATs, α-phellandrene (KMW0198) is positively regulated by 24 TFs (4 AP2/ERFs, 4 bHLHs, 3 bZIPs, 6 MYBs, 5 NACs, 2 WRKYs) and 2 terpenoid synthase genes (*TPS7* and *TPS5-10*) (Fig. 8C). These findings provide valuable information for the genetic control of volatile terpenoid synthesis in *A. tsao-ko*.

Discussion

Analysis of volatile organic compounds in differently shaped *A. tsao-ko* fruits

The types and contents of volatile metabolites play crucial roles in the medicinal uses and condiments of *A. tsao-ko*. Previous studies have primarily focused on the extraction and detection of volatile oils from *A. tsao-ko*. However, owing to technological limitations, the detection of volatile substances has been limited, hindering a comprehensive understanding of the volatile substances in *A. tsao-ko*. Additionally, there is limited knowledge regarding the variations in the VOC profiles of different *A. tsao-ko* fruit shapes. To address this gap, we utilized a newly developed WTV technique to detect 978 volatile metabolites. Among these, 971 were identified in L1, 976 in O1, 963 in R1, 976 in L2, 968 in O2, and 971 in R2. These findings significantly surpassed the number of previously reported metabolites [3]. In addition to the previously mentioned terpenoids, a significant number of esters, heterocyclic compounds, ketones, alcohols, hydrocarbons, aldehydes, and aromatic hydrocarbons were detected. This study expands our understanding of the volatile metabolic profile of *A. tsao-ko* and establishes a solid foundation for future research on functional substances and quality improvement. Notably, eucalyptol and β-phellandrene were found to be highly abundant in all six groups of samples, indicating their importance as VOCs in *A. tsao-ko*. Eucalyptol has a long history of use in traditional medicine and exhibits various biological properties, including anti-inflammatory, antioxidant, antimicrobial, bronchodilator, analgesic, and pro-apoptotic properties [23, 24]. Previous research has also suggested that β-phellandrene may possess antimicrobial and antifungal effects in grapefruit [25], and it can be utilized as an insect repellent and insecticide [26].

Terpenoids, the main active ingredients in *A. tsao-ko*, have the largest number and highest content among the volatile substances. In fresh fruits, 40 significantly differential terpenoids were identified, including high-content terpenoids such as pseudolimonene, β-pinene, α-phellandrene, sabinene, β-elemene, and terpinolene. Notably, α-phellandrene showed significant differences among the different fruit shapes, with its highest relative content being in L1 (1549.01 μg/g), which was 3.01 times that in O1 and 49.68 times that in R1. Previous studies have demonstrated that α-phellandrene exerts antitumor, antinociceptive, larvicidal, and insecticidal activities [27]. Additionally, terpinolene also exhibited significant differences among the three fruit types, with its content in L1 (684.19 μg/g) being greater than that in O1 (207.91 μg/g) and R1 (67.60 μg/g). Terpinolene possesses antioxidant, antifungal, insecticidal, larvicidal, anti-inflammatory, and antitumor effects [28]. β-pinene, a key component in *A. tsao-ko*'s volatile oil, has diverse pharmacological effects [29]. This study found a significant difference in β-pinene content between L1 and R1, with L1 having more. O1 had higher levels of sabinene and β-elemene, while R1 had more (+)-limonene oxide and (Z)-2,2-Dimethyl-3-(3-methylpenta-2,4-dien-1-yl)oxirane. The varying volatile aroma components from different fruit shapes define their unique scents. Interestingly, there are still significant differences in α-phellandrene in different fruit shapes after drying. Considering the importance of α-phellandrene, it can serve as signature metabolites for identifying different fruit types.

The fresh fruit of *A. tsao-ko* has a distinct, fresh, spicy, and pungent odor. However, when dried, the spicy and pungent odor decreases, and its aroma and sweetness increase. Previous studies have focused on analyzing small compounds, such as aldehydes, pyrazines, pyrroles, furans, ketones, acids, and alcohols, which contribute to the formation of aroma in malt [30]. Ketones are commonly associated with pungent smells, whereas esters are known for their floral, fruity and spicy notes. In the present study, we observed significant changes in the levels of multiple VOCs before and after drying *A. tsao-ko*. Specifically, 78 DAVOCs were common among the three fruit shapes. The contents of (E)-2-hexenal, which imparts a grassy and fresh aroma, and 4-hexen-3-one, which is known for its green and pungent spicy flavor, were significantly reduced in the dried fruit. The abundance of several VOCs related to aroma and sweetness was significantly increased, including that of cinnamic acid (balsamic, sweet, storax), a,a-dimethylphenethyl butyrate (floral, fruity), (-)-borneol (pine, woody, camphor), 4-pentenyl acetate (cooked meat), (6Z)-nonen-1-ol (pine, woody, camphor), ethyl cyclohexanepropionate (fruity, sweet, pineapple, peach, pear), and isomaltol (burnt, caramel, fruity) [31]. (-)-borneol, a bicyclic monoterpenoid, exhibits a wide range of biological activities. Notably, 2-pentyl-2-cyclopenten-1-one was only detected in the dried fruits of *A. tsao-ko* and is known to enhance floral aromas in flavor preparations [32].

Mining of volatile terpenoid metabolism genes

Terpenoids are synthesized via the MVA and MEP pathways. The MVA pathway primarily synthesizes sesquiterpenes, whereas the MEP pathway is responsible for the biosynthesis of monoterpenes and diterpenes [33]. The MVA and MEP pathways are not completely independent, and there is crosstalk between them [34–36]. However, limited information is available regarding the biosynthetic pathways of volatile terpenoids in *A. tsao-ko*, particularly regarding the identification of key genes involved in the formation of differential volatiles in different fruit types. To address this knowledge gap, we conducted a comprehensive analysis to investigate the expression patterns of genes involved in the volatile

terpenoid pathway in *A. tsao-ko*. We identified 40 structural genes, including 18 terpenoid skeleton and 22 terpenoid synthase genes, through transcriptomic data. These genes encompassed key enzymes such as *HMGS*, *HMGR*, and *FPPS* from the MVA pathway and *DXS*, *DXR*, *ispG*, and *ispH* from the MEP pathway. The differential expression of these genes was observed in relation to the different fruit shapes. *HMGR-2*, an important rate-limiting enzyme in the MVA pathway, showed a significant positive correlation with three sesquiterpenes (petasitene, β-elemene, and Bicyclo[5.2.0]nonane, 2-methylene-4,8,8-trimethyl-4-vinyl-) as well as the monoterpene (-)-borneol. A similar regulation of monoterpene synthesis by *HMGR* has been reported in other plant species, such as *Camphor Tulsi* [37], grape [38, 39], and lilac [40]. Two differentially expressed monoterpene synthase genes, *TPS7* and *TPS8* were identified by WGCNA. *TPS7* shares the highest homology with the bornyl *diphosphate synthase* (*BPPS*) gene in *Amomum villosum*. It is a multiproduct enzyme and showed a positive correlation with nine monoterpenoids, including bornyl acetate, D-limonene, β-pinene, and α-phellandrene [41]. In the present study, *TPS7* exhibited a highly significant positive correlation with three monoterpenes: terpinolene, pseudolimonene, and α-phellandrene. *TPS5-10* showed a significant positive correlation with four monoterpenes (pseudolimonene, α-phellandrene, terpinolene, and β-pinene) and one sesquiterpene (δ-elemene), indicating its dual function in synthesizing both monoterpenes and sesquiterpenes. *TPS5-10* is annotated as a nerolidol synthase and is a multiproduct terpenoid synthase that exhibits bifunctionality in the synthesis of both monoterpenes and sesquiterpenes [42, 43]. Additionally, we identified two sesquiterpene synthase genes, *TPS21-6* and *TPS21-7*, which were significantly positively correlated with three sesquiterpenes: Bicyclo[5.2.0]nonane, 2-methylene-4,8,8-trimethyl-4-vinyl-, petasitene, and β-elemene. These two genes could play crucial roles in sesquiterpenoid synthesis in *A. tsao-ko*.

In plants, terpenoid synthesis is primarily regulated by transcription factors. Six main transcription factor families involved in terpenoid metabolism have been identified (AP2/ERF, bHLH, MYB, NAC, WRKY, and bZIP) [21]. In *D. chrysotoxum*, ERF, NAC, WRKY, and MYB have been found to play crucial roles in the biosynthesis of the terpenoid skeleton during the flowering stage [17]. Similarly, in *A. tsao-ko*, four WRKYs, three MYBs, three bHLHs, one NAC, and one bZIP are highly correlated with eight terpenoids [6]. In tea, MYB, NAC, ERF, WRKY, and bHLH are significantly correlated with the expression of key genes involved in the terpenoid biosynthesis pathway [44]. The synthesis of linalool, a flavor-related compound, is regulated by *PpbHLH1* during peach fruit development [45]. NAC transcription factors also play an important role in regulating monoterpene production during kiwifruit ripening [46]. Suttipanta et al. [47] discovered that the overexpression of *Cr-WRKY1* in *Catharanthus roseus* could downregulate the expression of *ORCA2/3*, *CrMYC2*, and *ZCTs*, thereby regulating the synthesis of monoterpenes. To elucidate the TFs potentially involved in the regulation of volatile terpenoid biosynthesis, we conducted WGCNA to identify key structural genes and TFs. Our analysis revealed that 81 TFs exhibited significant correlations with 19 DATs, including 16 AP2/ERFs, 13 bHLHs, 6 bZIPs, 16 MYBs, 17 NACs, and 13 WRKYs. We propose that these TFs may bind to the promoters of key genes, thereby playing crucial roles in the regulation of volatile terpenoid synthesis. Specifically, *TPS7* and *TPS5-10*, which demonstrate significant positive correlations with α-phellandrene, pseudolimonene, and terpinolene, are co-expressed with 24 TFs. Furthermore, *HMGR-2*, *TPS21-6*, and *TPS21-7*, which are involved in sesquiterpene synthesis, exhibit similar expression patterns with 21 TFs, including seven MYBs (*MYB1*, *MYB2*, *MYB3*, *MYB4*, *MYB12*, *MYB13*, and *MYB14*). Previous studies have demonstrated that MYB transcription factors regulate sesquiterpene synthesis in *Pogostemon cablin* [48], tomato [49], *Dendrobium officinale* [50], and conifer trees [51]. This study provides new insights into the molecular mechanisms underlying volatile terpenoid biosynthesis in *A. tsao-ko*.

Conclusion

In conclusion, WTV methods were used to investigate the VOCs in three differently shaped *A. tsao-ko* fruits (long, oval, and round) before and after drying. A total of 978 VOCs were identified, with terpenoids emerging as the predominant compounds. The DAVOCs across comparison groups mainly consist of heterocyclic compounds, terpenoids, and esters. Additionally, 78 shared DAVOCs were identified before and after the drying, which were pivotal in contributing to the aromatic distinctions between the fresh and dried fruits. Moreover, our WGCNA analyses revealed that 19 DATs were significantly associated with 8 structural genes, including *HMGR-2*, *TPS7*, *TPS5-10*, *TPS21-3*, *TPS21-5*, *TPS21-6*, *TPS21-7*, and *TPS21-9*. Meanwhile, 81 candidate transcription factor genes related to volatile terpenoid biosynthesis, including NACs, MYBs, AP2/ERFs, WRKYs, bHLHs, and bZIPs, exhibited significant correlations with the DATs. This study expands our understanding of volatile metabolism in *A. tsao-ko*, elucidated the variations in VOCs among differently shaped *A. tsao-ko* fruits, and identified several genes associated with terpenoid metabolism. Our findings therefore provide a solid foundation for improving the quality of *A. tsao-ko*.

Abbreviations

VOCs	Volatile organic compounds
DAVOCs	Differentially accumulated volatile organic compounds
DATs	Differentially accumulated terpenoids
MVA	Mevalonic acid
MEP	2-c-methylerythritol 4-phosphate
GC–MS	Gas chromatography–mass spectrometry
WTV	Widely targeted volatilomics
LWR	Length-to-width ratio
SPME	Headspace solid-phase microextraction
OPLS-DA	Orthogonal partial least squares discriminant analysis
VIP	Variable importance in projection
FPKM	Fragments per kilobase of transcript per million mapped reads
DEGs	Differentially expressed genes
KEGG	Kyoto encyclopedia of genes and genomes
WGCNA	Weighted gene co-expression network analysis

Supplementary Information

The online version contains supplementary material available at https://doi.org/10.1186/s12870-024-05594-4.

Supplementary Material 1

Acknowledgements
We would like to thank Editage (www.editage.cn) for English language editing.

Author contributions
B.L. conceived and designed the experiments; B.L., T.W., and P.F. collected *A. tsao-ko* samples; M.M., H.F., and L.X. performed the experiments; B.L., and M.M. analyzed the data and wrote the manuscript. All authors reviewed and approved the manuscript.

Funding
This work was supported by the National Natural Science Foundation of China (Grant No. NSFC- No. 82260735, 31460380), the Youth Top-notch Talent Support Program of Yunnan Province (No. YNWR–QNBJ–2020–207), the Special Basic Cooperative Research Programs of Yunnan Provincial Undergraduate Universities' Association (No. 202001BA070001–181, 202101BA070001-180), and the Scientific Research Fund of the Yunnan Provincial Education Department (No. 2021J0545).

Data availability
The original sequencing data generated in the study have been deposited into the National Center for Biotechnology Information (NCBI) Sequence Read Archive (SRA) database with the primary accession code PRJNA1072740, other datasets supporting the conclusions of this article are included within the manuscript or supplementary information files.

Declarations

Ethics approval and consent to participate
Amomum tsao-ko is neither wild nor endangered in China, and no specific permission was required for the collection. The study complied with relevant institutional, national, and international guidelines and legislation.

Consent for publication
Not applicable.

Competing interests
The authors declare no competing interests.

Received: 25 June 2024 / Accepted: 13 September 2024
Published online: 01 October 2024

References

1. Ma ML, Meng HL, Lei E, Wang TT, Zhang W, Lu BY. De novo transcriptome assembly, gene annotation, and EST-SSR marker development of an important medicinal and edible crop, *Amomum tsaoko* (Zingiberaceae). BMC Plant Biol. 2022;22(1):467.
2. Yang SY, Xue YF, Chen DJ, Wang ZT. *Amomum tsao-ko* Crevost & Lemarié: a comprehensive review on traditional uses, botany, phytochemistry, and pharmacology. Phytochem Rev. 2022;21(5):1487–521.
3. He G, Yang SB, Wang YZ. The potential of *Amomum tsao-ko* as a traditional Chinese medicine: traditional clinical applications, phytochemistry and pharmacological properties. Arab J Chem. 2023;16(8):104936.
4. Lu BY, Ma ML, Wang TT, Meng HL, Lei E, Zhang W. Genetic diversity and genetic relationships of *Amomum tsao-ko* based on random amplified polymorphic DNA markers. Int J Agric Biol. 2018;20(9):2032–8.
5. Li GD, Lu QW, Wang JJ, Hu QY, Liu PH, Yang YW, Li YK, Tang HR, Xie H. Correlation analysis of aompounds in essential oil of *Amomum Tsaoko* seed and fruit morphological characteristics, geographical conditions, locality of growth. Agronomy. 2021;11(4):744.
6. Li P, Bai GX, He JB, Liu B, Long JR, Morcol T, Peng WY, Quan F, Luan XB, Wang ZZ, et al. Chromosome-level genome assembly of *Amomum tsao-ko* provides insights into the biosynthesis of flavor compounds. Hortic Res. 2022;9:uhac211.
7. Pu ZH, Wang BS, Zhang SY, Sun FH, Dai M. A review on quality control, toxicity and clinical application of *Amomum tsao-ko* Crevost & Lemarié. Pharmacol Res - Mod Chin Med. 2022;5:100165.
8. Cox-Georgian D, Ramadoss N, Dona C, Basu C. Therapeutic and medicinal uses of terpenes. In: *Medicinal Plants: From Farm to Pharmacy.* Edited by Joshee N, Dhekney SA, Parajuli P. Cham: Springer International Publishing; 2019: 333–359.
9. Sun FH, Yan CC, Lv YY, Pu ZH, Liao ZD, Guo W, Dai M. Genome sequencing of *Amomum tsao-ko* provides novel insight into tts volatile component biosynthesis. Front Plant Sci. 2022;13:904178.
10. Cui Q, Wang LT, Liu JZ, Wang HM, Guo N, Gu CB, Fu YJ. Rapid extraction of *Amomum tsao-ko* essential oil and determination of its chemical composition, antioxidant and antimicrobial activities. J Chromatogr B. 2017;1061–1062:364–71.
11. Yang Y, Yan RW, Cai XQ, Zheng ZL, Zou GL. Chemical composition and antimicrobial activity of the essential oil of *Amomum tsao-ko*. J Sci Food Agric. 2008;88(12):2111–6.
12. Wang Y, You CX, Wang CF, Yang K, Chen R, Zhang WJ, Du SS, Geng ZF, Deng ZW. Chemical constituents and insecticidal activities of the essential oil from *Amomum tsaoko* against two stored-product insects. J Oleo Sci. 2014;63(10):1019–26.
13. Yuan HL, Cao GP, Hou XD, Huang ML, Du PM, Tan TT, Zhang YJ, Zhou HH, Liu XQ, Liu L, et al. Development of a widely targeted volatilomics method for profiling volatilomes in plants. Mol Plant. 2022;15(1):189–202.
14. Yao HB, Su H, Ma JY, Zheng J, He W, Wu CL, Hou ZY, Zhao RL, Zhou QQ. Widely targeted volatileomics analysis reveals the typical aroma formation of Xinyang black tea during fermentation. Food Res Int. 2023;164:112387.
15. Zhang C, Zhou CZ, Xu K, Tian CY, Zhang MC, Lu L, Zhu C, Lai ZX, Guo YQ. A comprehensive investigation of macro-composition and volatile compounds in spring-picked and autumn-picked white tea. Foods. 2022;11(22):3628.
16. Liu H, Chen WD, Chai YH, Liu WC, Chen HX, Sun L, Tang XW, Luo C, Chen DL, Cheng X et al. Terpenoids and their gene regulatory networks in *Opisthopappus taihangensis* 'Taihang Mingzhu' as detected by transcriptome and metabolome analyses. Front Plant Sci 2022;13:1014114.
17. Du ZH, Jin YX, Wang WZ, Xia KF, Chen ZL. Molecular and metabolic insights into floral scent biosynthesis during flowering in *Dendrobium Chrysotoxum*. Front Plant Sci 2022;13:1030492.
18. Fang X, Xu WC, Jiang GX, Sui MY, Xiao JY, Ning YY, Niaz R, Wu DW, Xu F, Chen JH, Huang YY, Lei GX. Monitoring the dynamic changes in aroma during the whole processing of Qingzhuan tea at an industrial scale: from fresh leaves to finished tea. Food Chem. 2024;439:137810.
19. Chen SF, Zhou YQ, Chen YR, Gu J. Fastp: an ultra-fast all-in-one FASTQ preprocessor. Bioinformatics. 2018;34(17):i884–90.
20. Kim D, Langmead B, Salzberg SL. HISAT: a fast spliced aligner with low memory requirements. Nat Methods. 2015;12(4):357–60.
21. Li B, Dewey CN. RSEM: accurate transcript quantification from RNA-Seq data with or without a reference genome. BMC Bioinformatics. 2011;12(1):323.
22. Dong YM, Zhang WY, Ling ZY, Li JR, Bai HT, Li H, Shi L. Advances in transcription factors regulating plant terpenoids biosynthesis. Chin Bull Bot. 2020;55(3):340–50.
23. Cai ZM, Peng JQ, Chen Y, Tao L, Zhang YY, Fu LY, Long QD, Shen XC. 1,8-Cineole: a review of source, biological activities, and application. J Asian Nat Prod Res. 2021;23(10):938–54.

24. Hoch CC, Petry J, Griesbaum L, Weiser T, Werner K, Ploch M, Verschoor A, Multhoff G, Bashiri Dezfouli A, Wollenberg B. 1,8-cineole (eucalyptol): a versatile phytochemical with therapeutic applications across multiple diseases. Biomed Pharmacother. 2023;167:115467.
25. Miya G, Nyalambisa M, Oyedeji O, Gondwe M, Oyedeji A. Chemical profiling, toxicity and anti-inflammatory activities of essential oils from three grapefruit cultivars from KwaZulu-Natal in South Africa. Molecules. 2021;26(11):3387.
26. Cao JQ, Pang X, Guo SS, Wang Y, Geng ZF, Sang YL, Guo PJ, Du SS. Pinene-rich essential oils from *Haplophyllum dauricum* (L.) G. Don display anti-insect activity on two stored-product insects. Int Biodeterior Biodegrad. 2019;140:1–8.
27. Radice M, Durofil A, Buzzi R, Baldini E, Martínez AP, Scalvenzi L, Manfredini S. Alpha-phellandrene and alpha-phellandrene-rich essential oils: a systematic review of biological activities, pharmaceutical and food applications. Life. 2022;12(10):1602.
28. Menezes IO, Scherf JR, Martins AOBPB, Ramos AGB, Quintans JSS, Coutinho HDM, Ribeiro-Filho J, de Menezes IRA. Biological properties of terpinolene evidenced by in silico, in vitro and in vivo studies: a systematic review. Phytomedicine. 2021;93:153768.
29. Salehi B, Upadhyay S, Erdogan Orhan I, Kumar Jugran A, Jayaweera LD, Dias SA, Sharopov D, Taheri F, Martins Y, Baghalpour N. Therapeutic potential of α-and β-pinene: a miracle gift of nature [J]. Biomolecules. 2019;9(11):738.
30. Prado R, Gastl M, Becker T. Aroma and color development during the production of specialty malts: a review. Compr Rev Food Sci Food Saf. 2021;20(5):4816–40.
31. Ma R, Lu DN, Wang J, Xie Q, Guo JL. Comparison of pharmacological activity and safety of different stereochemical configurations of borneol: L-borneol, D-borneol, and synthetic borneol. Biomed Pharmacother. 2023;164:114668.
32. Lu Z. Simultaneous determination of three prohibited substances in fragrance compound through gas chromatography-mass spectrometry. Food Mach. 2018;34(6):55–7.
33. Abbas F, Ke YG, Yu RC, Yue YC, Amanullah S, Jahangir MM, Fan YP. Volatile terpenoids: multiple functions, biosynthesis, modulation and manipulation by genetic engineering. Planta. 2017;246(5):803–16.
34. Laule O, Fürholz A, Chang HS, Zhu T, Wang X, Heifetz PB, Gruissem W, Lange M. Crosstalk between cytosolic and plastidial pathways of isoprenoid biosynthesis in *Arabidopsis thaliana*. Proc Natl Acad Sci. 2003;100(11):6866–71.
35. Mendoza-Poudereux I, Kutzner E, Huber C, Segura J, Eisenreich W, Arrillaga I. Metabolic cross-talk between pathways of terpenoid backbone biosynthesis in spike lavender. Plant Physiol Biochem. 2015;95:113–20.
36. Xu QS, He YX, Yan XM, Zhao SQ, Zhu JY, Wei CL. Unraveling a crosstalk regulatory network of temporal aroma accumulation in tea plant (*Camellia sinensis*) leaves by integration of metabolomics and transcriptomics. Environ Exp Bot. 2018;149:81–94.
37. Bansal S, Narnoliya LK, Mishra B, Chandra M, Yadav RK, Sangwan NS. HMG-CoA reductase from Camphor Tulsi (*Ocimum kilimandscharicum*) regulated MVA dependent biosynthesis of diverse terpenoids in homologous and heterologous plant systems. Sci Rep. 2018;8(1):3547.
38. Leng XP, Cong JM, Cheng LX, Wan HL, Liu YX, Yuan YB, Fang JG. Identification of key gene networks controlling monoterpene biosynthesis during grape ripening by integrating transcriptome and metabolite profiling. Hortic Plant J. 2023;9(5):931–46.
39. Li W, Li WF, Yang SJ, Ma ZH, Zhou Q, Mao J, Han SY, Chen BH. Transcriptome and metabolite conjoint analysis reveals that exogenous methyl jasmonate regulates monoterpene synthesis in grape berry skin. J Agric Food Chem. 2020;68(18):5270–81.
40. Yang ZY, Zhu YY, Zhang X, Zhang HL, Zhang XY, Liu GZ, Zhao QZ, Bao ZL, Ma FF. Volatile secondary metabolome and transcriptome analysis reveals distinct regulation mechanism of aroma biosynthesis in *Syringa oblata* and *S. Vulgaris*. Plant Physiol Biochem. 2023;196:965–73.
41. Wang H, Ma DM, Yang JF, Deng K, Li M, Ji XY, Zhong LT, Zhao HY. An integrative volatile terpenoid profiling and transcriptomics analysis for gene mining and functional characterization of *AvBPPS* and *AvPS* involved in the monoterpenoid biosynthesis in *Amomum Villosum*. Front Plant Sci. 2018;9:846.
42. Ibdah M, Hino S, Nawade B, Yahyaa M, Bosamia TC, Shaltiel-Harpaz L. Identification and characterization of three nearly identical linalool/nerolidol synthase from *Acorus calamus*. Phytochemistry. 2022;202:113318.
43. Qiao DH, Tang MS, Jin L, Mi XZ, Chen HR, Zhu JY, Liu SR, Wei CL. A monoterpene synthase gene cluster of tea plant (*Camellia sinensis*) potentially involved in constitutive and herbivore-induced terpene formation. Plant Physiol Biochem. 2022;184:1–13.
44. Qiao DH, Mi XZ, An YL, Xie H, Cao KM, Chen HR, Chen MY, Liu SR, Chen J, Wei CL. Integrated metabolic phenotypes and gene expression profiles revealed the effect of spreading on aroma volatiles formation in postharvest leaves of green tea. Food Res Int. 2021;149:110680.
45. Wei CY, Liu HR, Cao XM, Zhang ML, Li X, Chen KS, Zhang B. Synthesis of flavour-related linalool is regulated by *PpbHLH1* and associated with changes in DNA methylation during peach fruit ripening. Plant Biotechnol J. 2021;19(10):2082–96.
46. Nieuwenhuizen NJ, Chen X, Wang MY, Matich AJ, Perez RL, Allan AC, Green SA, Atkinson RG. Natural variation in monoterpene synthesis in kiwifruit: transcriptional regulation of terpene synthases by NAC and ETHYLENE-INSENSITIVE3-like transcription factors. Plant Physiol. 2015;167(4):1243–58.
47. Suttipanta N, Pattanaik S, Kulshrestha M, Patra B, Singh SK, Yuan L. The transcription factor CrWRKY1 positively regulates the terpenoid indole alkaloid biosynthesis in *Catharanthus roseus*. Plant Physiol. 2011;157(4):2081–93.
48. Chen XZ, Li JR, Liu YT, Wu DD, Huang HL, Zhan RT, Chen WW, Chen LK. PatSWC4, a methyl jasmonate-responsive MYB (v-myb avian myeloblastosis viral oncogene homolog)-related transcription factor, positively regulates patchoulol biosynthesis in *Pogostemon cablin*. Ind Crops Prod. 2020;154:112672.
49. Gong ZH, Luo YQ, Zhang WF, Jian W, Zhang L, Gao XL, Hu XW, Yuan YJ, Wu MB, Xu X, et al. A SlMYB75-centred transcriptional cascade regulates trichome formation and sesquiterpene accumulation in tomato. J Exp Bot. 2021;72(10):3806–20.
50. Lv M, Sun X, Li DC, Wei G, Liu L, Chen F, Cai YP, Fan HH. Terpenoid biosynthesis in *Dendrobium officinale*: identification of (*E*)-β-caryophyllene synthase and the regulatory *MYB* genes. Ind Crops Prod. 2022;182:114875.
51. Bedon F, Bomal C, Caron S, Levasseur C, Boyle B, Mansfield SD, Schmidt A, Gershenzon J, Grima-Pettenati J, Séguin A, et al. Subgroup 4 R2R3-MYBs in conifer trees: gene family expansion and contribution to the isoprenoid- and flavonoid-oriented responses. J Exp Bot. 2010;61(14):3847–64.

Publisher's note